

1 **Type I phosphatidylinositol-4-phosphate 5-kinase α and γ play a key role in targeting**
2 **HIV-1 Pr55^{Gag} to the plasma membrane**

3
4
5 Baptiste Gonzales,^a Hugues de Rocquigny,^a Anne Beziau,^a Stephanie Durand,^a Julien Burlaud-Gaillard,^a
6 Antoine Lefebvre,^b Sandra Krull,^c Patrick Emond^b, Denys Brand,^{a,c} Eric Piver^{a,c#}

7
8
9 ^aINSERM U1259, University of Tours, France

10 ^bINSERM U1253, University of Tours, France

11 ^cBiochimie et Biologie Moléculaire, Tours University Hospital, France

12 ^dLaboratoire de Virologie, Tours University Hospital, France

13 ^eMax Delbrueck Center for Molecular Medicine, Berlin, Germany

14
15
16
17 Running Head: HIV, PIP5K1, Pr55^{Gag}, plasma membrane targeting.

18
19
20
21
22
23 Word count for the abstract: 210

24 Word count for the text (excluding the references, table footnotes, and figure legends): 5561

25
26
27
28
29
30
31
32
33
34 #Address correspondence to Eric Piver, piver_e@univ-tours.fr

37 **Abstract**

38 HIV-1 assembly occurs principally at the plasma membrane (PM) of infected cells. Gag
39 polyprotein precursors (Pr55^{Gag}) are targeted to the PM and their binding is mediated by the
40 interaction of myristoylated matrix domain and a PM-specific phosphoinositide, the
41 phosphatidylinositol-(4,5)-bisphosphate (PI(4,5)P₂). The major synthesis pathway of PI(4,5)P₂
42 involves the activity of phosphatidylinositol 4-phosphate 5-kinase family type 1 composed of
43 three isoforms (PIP5K1 α , β and γ). To examine whether the activity of a specific PIP5K1
44 isoform determines proper Pr55^{Gag} localization at the PM, we compared cellular behavior of
45 Pr55^{Gag} in the context of PIP5K1 inhibition using siRNAs that individually targeted each of the
46 three isoforms in TZM-bl HeLa cells. We found that downregulation of PIP5K1 α and PIP5K1 γ
47 strongly impaired the targeting of Pr55^{Gag} to the PM with a rerouting of the polyprotein within
48 intracellular compartments. The efficiency of Pr55^{Gag} release was thus impaired through the
49 silencing of these two isoforms while PIP5K1 β is dispensable for Pr55^{Gag} targeting to PM. The
50 PM-mistargeting due to the silencing of PIP5K1 α leads to Pr55^{Gag} hydrolysis through lysosome
51 and proteasome pathways while the silencing of PIP5K1 γ leads to Pr55^{Gag} accumulation in late
52 endosomes. Our findings demonstrated that, within the PIP5K1s family, only the PI(4,5)P₂
53 pools produced by PIP5K1 α and γ are involved in Pr55^{Gag} PM targeting process.

54

55 **Importance**

56 PM specificity of Pr55^{Gag} membrane binding is mediated through the interaction of PI(4,5)P₂
57 with the MA basic residues. It was shown that overexpression of a PI(4,5)P₂-depleting enzyme
58 strongly impaired plasma membrane (PM) localization of Pr55^{Gag}. However, cellular factors
59 that control PI(4,5)P₂-production required for Pr55^{Gag}-PM targeting have not yet been
60 characterized. In this study, by individually inhibiting PIP5K1 isoforms, we elucidated a
61 correlation between PI(4,5)P₂-metabolism pathways mediated by PIP5K1 isoforms and the

62 targeting of Pr55^{Gag} to the PM of TZM-bl HeLa cells. Confocal microscopy analyses of cells
63 depleted from PIP5K1 α and γ show a rerouting of Pr55^{Gag} to various intracellular
64 compartments. Notably, Pr55^{Gag} is degraded by the proteasome and/or by the lysosomes in
65 PIP5K1 α -depleted cells while Pr55^{Gag} is targeted to endosomal vesicles in PIP5K1 γ -depleted
66 cells. Thus, our results highlight for the first time the roles of PIP5K1 α and γ as determinants
67 of Pr55^{Gag} targeting to the PM.

68

69

70

71

72

73

74

75

76

77

78

79

80

81

82

83 Introduction

84 Human immunodeficiency virus type 1 (HIV-1) assembly, budding and release involve a highly
85 orchestrated series of interactions between the viral RNA, viral proteins and host factors of the
86 plasma membrane (PM). These late steps of the viral replication cycle are coordinated by the
87 Gag precursor (Pr55^{Gag}) and are initiated by the targeting of Pr55^{Gag} complexes to the inner
88 leaflet of the PM (1). Pr55^{Gag} contains three major structural domains — the matrix (MA),
89 capsid (CA) and nucleocapsid (NC) domains — together with two spacer peptides (sp1 and
90 sp2) and an unstructured C-terminal p6 peptide (2). The N-terminal MA domain targets Pr55^{Gag}
91 to the PM *via* two specific motifs: an N-terminal myristoyl moiety and a highly basic region
92 (HBR) spanning residues 17 to 31 (3–5). Pr55^{Gag} targeting to the PM is dependent on the
93 binding of MA HBR to phosphatidylinositol-4,5-biphosphate (PI(4,5)P₂) (6–10). The
94 electrostatic interactions of Pr55^{Gag} with PI(4,5)P₂ at the PM, together with the initiation of
95 Pr55^{Gag} multimerization, expose the N-terminal myristoyl moiety outside its hydrophobic
96 pocket, thereby reinforcing the Pr55^{Gag}-PM association driven by the HBR (10–13).

97 The principal mechanism of PI(4,5)P₂ production is the phosphorylation of
98 phosphatidylinositol-4-monophosphate (PI(4)P), at the D5 position of the inositol ring, by
99 phosphatidylinositol-4-phosphate 5-kinase family type 1 (PIP5K1). The PIP5K1s family
100 includes three isoforms (α , β , γ) with unique tissue distributions, present in different subcellular
101 compartments and generating functionally different specialized pools of PI(4,5)P₂ (14).
102 PIP5K1 α has been detected in different subcellular compartments, including the Golgi
103 compartment, PM and nuclei, in which it produces the PI(4,5)P₂ involved in reorganization of
104 the actin cytoskeleton, membrane ruffle formation and pre-mRNA splicing (14–18). PIP5K1 α
105 activity, which is controlled by Arf6, is also crucial for trafficking through the Arf6 PM-
106 endosomal recycling pathway (19). PIP5K1 β is localized to vesicular structures in the
107 perinuclear region, in which the PI(4,5)P₂ pool may be involved in actin dynamics and

108 endocytosis (14, 18). Finally, the PIP5K1 γ isoform has six splice variants, named PIP5K1 γ -v1–
109 6 (18, 20, 21). PIP5K1 γ proteins are preferentially localized to the PM, cell-cell junctions or
110 focal adhesions (18, 22–24). They are involved in various signaling processes, including the
111 production of the PI(4,5)P₂ pool used to generate inositol 3-phosphate (InsP₃), which is
112 involved in Ca²⁺ efflux and secretion (25).

113 PI(4,5)P₂ was shown to be essential for the targeting of Pr55^{Gag} to the PM in studies using
114 phosphoinositide 5-phosphatase IV, which depletes the cell of PI(4,5)P₂, causing the retargeting
115 of Pr55^{Gag} to late endosomes (6). More recently, the manipulation of PI(4,5)P₂ levels was shown
116 to prevent the correct targeting of Pr55^{Gag} to the PM and to cause the loss of pre-assembled
117 Pr55^{Gag} lattice from the PM (12). However, both these approaches deplete all PI(4,5)P₂ pools,
118 regardless of PIP5Ks isoforms implication in PI(4,5)P₂ metabolism. We investigated the role
119 of PI(4,5)P₂ in the targeting of Pr55^{Gag} to the PM inner leaflet in more detail, by focusing on
120 the cellular activity of PIP5Ks type 1 to study the effect of PI(4,5)P₂ metabolism on the
121 intracellular distribution of Pr55^{Gag}.

122 To address this question, we transfected TZM-bl HeLa cells with siRNAs targeting the various
123 PIP5K1 isoforms (α , β and γ). The decrease in total cellular PI(4,5)P₂ through PIP5K1 silencing
124 was assessed by ultra-high pressure liquid chromatography coupled with high-resolution mass
125 spectrometry (UHPLC-HRMS²). This method made a semi-quantitative analysis of the
126 distribution of PI(4,5)P₂ molecular species possible. PIP5K1 silencing led to a decrease in total
127 cellular PI(4,5)P₂ levels, and this effect was particularly strong for PIP5K1 α silencing. We then
128 showed that the silencing of PIP5K1 α or γ decreased the accumulation of Pr55^{Gag} at the PM
129 while the silencing of PIP5K1 β had no effect. The PM-mistargeting due to the silencing of
130 PIP5K1 α led to Pr55^{Gag} hydrolysis through lysosome and proteasome pathways while the
131 silencing of PIP5K1 γ led to Pr55^{Gag} accumulation in late endosomes. The disruption of these

132 two pathways of PI(4,5)P₂ metabolism was thus found to alter the extracellular release of
133 Pr55^{Gag}.

134

135 **Results**

136 **The silencing of PIP5K1 isoforms decreases PI(4,5)P₂ production.**

137 For identification of the PIP5K1 isoform involved in targeting Pr55^{Gag} to the PM, we
138 individually knocked down the expression of PIP5K1 α , β and γ . We therefore transfected TZM-
139 bl HeLa cells with siRNA mixtures or with untargeted siRNA as a control and the absolute
140 number of copies of targeted messenger RNA was determined by RT-qPCR 72 h post
141 transfection. The basal level of PIP5K1 α mRNA was approximately seven times higher than
142 those of PIP5K1 β and PIP5K1 γ (Fig. 1A, dark gray bars). PIP5K1 silencing decreased the
143 amounts of the PIP5K1 α , β and γ mRNAs by 80 \pm 12%, 70 \pm 7% and 76 \pm 10%, respectively (Fig.
144 1A, dashed bars). Consistent with this decrease, the levels of the corresponding protein isoforms
145 were about 70 to 80% lower than those in control cells (Fig. 1B). An additional faint band,
146 migrating slightly slower than the PIP5K1, was observed in Western blots using the PIP5K1 α
147 and β antibodies, which may correspond to an unspecific binding of the antibodies (26). Note
148 that the antibodies used here for the Western blot analysis were found inefficient for
149 immunofluorescence staining. The effect of each PIP5K1 isoform RNA knockdown on their
150 PIP5K1 RNA counterparts was also checked (Fig. 1C). Only the PIP5K1 α mRNA was shown
151 to be affected significantly, albeit weakly, in the context of siRNAs targeting PIP5K1 β or
152 PIP5K1 γ (Fig. 1C, grey and green bars). However, PIP5K1 β or γ mRNAs represent only ~15%
153 of the overall PIP5K1 RNAs (Fig. 1A). Therefore, we assumed that the effect of PIP5K1 α RNA
154 knockdown on Pr55^{Gag} subcellular localization was mostly linked to this isoform enzymatic
155 activity.

156 We next investigated the impact of PIP5K1 isoform silencing on PI(4,5)P₂ production, by

157 extracting lipids from siRNA-transfected cells. The concentrations of PI(4,5)P₂ and its various
158 fatty-acyl species were determined by UHPLC-HRMS². The addition of a known amount of
159 PI(4,5)P₂ internal standard (C16:0/C16:0) before lipid extraction made it possible to estimate
160 the amount of PI(4,5)P₂ total pool. The knockdown of PIP5K1 α decreased the amount of
161 PI(4,5)P₂ by 70 \pm 9% (Fig. 1D, blue bar) relative to the amount in experiments with non-targeting
162 control siRNA (Fig. 1D, black bar), whereas the silencing of PIP5K1 β and PIP5K1 γ decreased
163 the amount of cellular PI(4,5)P₂ by 45 \pm 8% and 44 \pm 12%, respectively (Fig. 1D gray and green
164 bars). Taking into account the weak proportion of PIP5K1 β and PIP5K1 γ RNAs (Fig. 1A), this
165 important decrease of PI(4,5)P₂ production was unexpected. Thus, the metabolic flux rate of
166 each PIP5K1 isoform does not seem to be directly correlated with its concentration, as
167 previously shown for other metabolic functions (27). Taken together, the higher amount of
168 RNA found for the α isoform and the larger drop of PI(4,5)P₂ observed after its silencing
169 suggest that this isoform produces most of the total cellular PI(4,5)P₂.

170

171 **The knockdown of PIP5K1 isoforms has various effects on the broad range of PI(4,5)P₂**
172 **species.**

173 We then investigated the impact of the silencing of the various PIP5K1 isoforms on the
174 distribution of various fatty-acyl PI(4,5)P₂ species. By UHPLC-HRMS², the most sensitive
175 tools to analyze this minor lipids family, we were able to identify 13 molecular species of
176 PI(4,5)P₂ (Fig. 2). The response ratio of these molecular species ranged from 0.4 for the
177 minority species 20:4/16:0 to 11.5 for the majority species 20:2/18:0 (Fig. 2, black bars). The
178 depletion of an individual isoform significantly altered the production of all the species
179 identified, with the exception of one of the minority species (C18:0/C16:0) identified in this
180 cell type. The knockdown of PIP5K1 α resulted in a sharp decrease in PI(4,5)P₂ levels,
181 particularly for molecular species bearing the C18:0 acyl chain and an unsaturated fatty acyl

182 chain (Fig. 2, blue bars). Indeed, the levels of the C20:1/C18:0; C18:1/C18:0; C22:2/C18:0 and
183 C20:2/C18:0 species were reduced by 6.5-, 5-, 4.5- and 3.5-fold, respectively (Fig. 2, compare
184 the blue bars with the black bars). By contrast, the silencing of PIP5K1 β (gray bars) and
185 PIP5K1 γ (green bars) had a lesser impact on the production of PI(4,5)P₂ molecular species. For
186 example, the knockdown of these two isoforms had no significant effect on the production of
187 the three species bearing the C20:4 fatty acyl chain. In addition, PIP5K1 β depletion did not
188 alter the basal expression of C18:1/C18:1 species (Fig. 2). Moreover, the production of the three
189 species bearing the C18:1 fatty acyl chain was more strongly affected by the knockdown of
190 PIP5K1 α than by the knockdown of PIP5K1 β and PIP5K1 γ . The distribution of PI(4,5)P₂
191 molecular species was similar in HeLa cells and TZM-bl HeLa modified cells (data not shown).
192 Our findings show that PIP5K1 α activity is involved in the metabolism of a large range of
193 PI(4,5)P₂ species, whereas the activities of PIP5K1 β and PIP5K1 γ have a more restricted
194 involvement in this metabolism, consistent with the finding that PIP5K1 α is responsible for
195 most PI(4,5)P₂ production (Fig. 1D). Thus, PIP5K1 α is the principal producer of PI(4,5)P₂ in
196 the context of TZM-bl HeLa cells.

197

198 **The knockdown of PIP5K1 α and PIP5K1 γ impairs HIV-1 Pr55^{Gag} targeting to the plasma** 199 **membrane.**

200 We investigated whether the silencing of each PIP5K1 isoform and the resulting PI(4,5)P₂
201 depletion led to HIV-1 Pr55^{Gag} mislocalization. We transfected TZM-bl HeLa cells with
202 siRNAs and then with a mixture of plasmids encoding Pr55^{Gag} and Pr55^{Gag-eGFP} for an additional
203 24 h. The cells were then stained with the dSQ12S probe to delineate the PM (28) and analyzed
204 by confocal microscopy. As shown in the upper row of figure 3A, Pr55^{Gag} was partially
205 distributed at the PM while the dSQ12S probe was uniformly delineating this PM. As a
206 consequence, a partial colocalization of Pr55^{Gag} and dSQ12S probe was observed with a yellow

207 staining (Fig. 3A, row a). Punctate staining corresponding to the accumulation of Pr55^{Gag} was
208 also observed in the cytoplasm. The overlap between the two fluorescent reporters was
209 calculated by the “Squassh” method, with double-labeling evaluated by calculating Pearson’s
210 correlation coefficients (R) across the whole image (29). Consistent with the yellow staining of
211 the merged image (Fig. 3A, row a, merge), the Pr55^{Gag} staining overlapped with staining for
212 the dSQ12S probe with $R \sim 0.5$ (Fig. 3B, black dots). In sharp contrast, the depletion of
213 PIP5K1 α and γ had a major impact on the distribution of Pr55^{Gag}, with an accumulation of the
214 viral protein in intracellular compartments (Fig. 3A, rows b and d). This accumulation resulted
215 in a loss of colocalization of the two reporters with $0.05 < R > 0.1$ (Fig. 3B, blue and green dots).
216 Conversely, the silencing of PIP5K1 β had no effect on the cellular distribution of Pr55^{Gag}, with
217 cells displaying the same R coefficient as cells transfected with the non-targeting control siRNA
218 (Fig. 3A, row c and Fig. 3B, grey dots). Similar results for the silencing of the various PIP5K1
219 isoforms were obtained when Pr55^{Gag} was expressed together with Pr55^{Gag} translated from the
220 pNL4.3 proviral construct, suggesting that the role of PIP5K1 in Pr55^{Gag} targeting is identical
221 when the full-length HIV-1_{NL4.3} provirus genome is transfected (Fig. 3C and D). Overall, these
222 results provide the first evidence of a role for the metabolism of PI(4,5)P₂ mediated by PIP5K1 α
223 and PIP5K1 γ in the accumulation of Pr55^{Gag} at the PM.

224

225 **The silencing of PIP5K1 α and PIP5K1 γ has different effects on the retargeting of HIV-1**
226 **Pr55^{Gag} to endosomal pathways.**

227 We then sought to identify the subcellular compartments to which Pr55^{Gag} was redirected in
228 cells depleted of PIP5K1 α or PIP5K1 γ . Among vesicular markers, Rab GTPases are widely
229 used to distinguish early or late endosomes and lysosomes (30). Rab 5 and Rab 7A are proteins
230 associated with early and late endosomal compartments, respectively (31). Thus, we transfected
231 siRNA-treated cells with plasmids encoding Pr55^{Gag}/Pr55^{Gag}-eGFP together with a plasmid

232 encoding mCherry-tagged versions of Rab5 (Fig. 4A) or Rab7A (Fig. 4C). In order to make a
233 comprehensive figure, only images corresponding to the overlay of green and red channels
234 (merged images) were presented in the figure 4. In cell expressing mCherry-Rab5, we found
235 that Pr55^{Gag} did not accumulate in early endosomes whether the cells were treated with the non-
236 targeting control siRNA or depleted from each PIP5K1 isoform (Fig. 4A and 4B). Likewise, in
237 cells expressing mCherry-Rab7A, we found that Pr55^{Gag} did not accumulate in late endosomes
238 in cells transfected with the non-targeting control siRNA or depleted of PIP5K1 β (Fig. 4C,
239 images a and c and Fig. 4D, black and grey dots). Conversely, following the depletion of
240 PIP5K1 α or γ , much less Pr55^{Gag} was detected at the PM (Fig. 3A and 3C, rows b and d), with
241 accumulation of internal yellowish vesicles in the cytoplasm (Fig. 4C, images b and d). A
242 quantification of the colocalization between Pr55^{Gag} and Rab7A following the depletion of
243 PIP5K1 α and γ showed a double-staining for Pr55^{Gag} and mCherry-Rab7A with $R \sim 0.25$ (Fig.
244 4D, blue and green dots). These observations strongly suggest that knocking down the
245 expression of PIP5K1 α and γ led to the specific accumulation of the Pr55^{Gag} precursor in late
246 endosomes, whereas the knockdown of PIP5K1 β had no impact on Pr55^{Gag} distribution.

247 We then investigated the endosomal pathways followed by the late endosomes containing
248 Pr55^{Gag}, using the LysoTracker probe, which stains lysosome vesicles. In cells treated with the
249 non-targeting control siRNA or depleted of the PIP5K1 β protein, a weak if any colocalization
250 between Pr55^{Gag} and the LysoTracker was observed (Fig. 4E, images a and c) giving rise to R
251 < 0.1 (Fig. 4F, black and grey dots). Intriguingly, the same absence of colocalization between
252 Pr55^{Gag} and LysoTracker staining was observed in cells depleted of PIP5K1 γ (Fig. 4E, image d
253 and Fig. 4F, green dots). By contrast, the depletion of PIP5K1 α induced a double-staining for
254 Pr55^{Gag} and the LysoTracker probe ($R \sim 0.29$) (Fig. 4F, blue dots), as shown by the yellow
255 staining in PIP5K1 α -depleted cells (Fig. 4E, image b). These data indicate that Pr55^{Gag} follows

256 the lysosomal pathway and that late endosomes containing Pr55^{Gag} fuse with the acidic vesicles
257 only after depletion of the PIP5K1 α isoform but not after depletion of the PIP5K1 γ isoform.

258

259 **Effects of PIP5K1 α and PIP5K1 γ silencing on Pr55^{Gag} release.**

260 We investigated the role of each PIP5K1 isoform on Pr55^{Gag} release by quantifying the level of
261 Pr55^{Gag} in cell lysate and supernatant of PIP5K1-depleted cells (Fig. 5). PIP5K1 α -depleted
262 cells had much lower levels of Pr55^{Gag} in the cytoplasm than control cells (Fig. 5A, red
263 rectangle in upper panel), whereas Pr55^{Gag} levels were similar to those in control cells for both
264 PIP5K1 β - and PIP5K1 γ -depleted cells (Fig. 5A, upper panel). The levels of Pr55^{Gag} in the
265 supernatant were lower than those recorded for control cells, by a factor of 3 for PIP5K1 α -
266 depleted cells and 1.5 for PIP5K1 γ -depleted cells, whereas levels of Pr55^{Gag} in the supernatant
267 were unaffected in PIP5K1 β -depleted cells (Fig. 5B, white bars). Thus, the treatment of cells
268 by siRNA against PIP5K1 α decreased the amount of cytoplasmic Pr55^{Gag} and its release while
269 the treatment of cells by siRNA against PIP5K1 γ decreased only the release of Pr55^{Gag}. Then,
270 the efficiency of Pr55^{Gag} release was calculated by dividing the amount of Pr55^{Gag} expression
271 in the supernatant by the total amount of Pr55^{Gag} expressed in both the supernatant and the cell
272 lysate. In PIP5K1 α - and PIP5K1 β -depleted cells, Pr55^{Gag} release efficiency was similar to that
273 recorded for non-targeting control siRNA-treated cells (Fig. 5C, second and third white bars).
274 By contrast, PIP5K1 γ depletion decreased Pr55^{Gag} release efficiency by one third (Fig. 5C,
275 fourth white bar).

276 To overcome Pr55^{Gag} hydrolysis, these experiments were repeated in the presence of MG132
277 proteasome inhibitor (Fig. 5A, lower panel). The addition of MG132 to PIP5K1 α -depleted cells
278 restored the amount of cytoplasmic Pr55^{Gag} almost to control levels (Fig. 5A, red rectangle in
279 lower panel). A similar result was obtained when the cells were treated with the lysosomal
280 inhibitor bafilomycin A1 (data not shown) (32). These observations confirmed that the

281 depletion of PIP5K1 α causes Pr55^{Gag} hydrolysis. Surprisingly, this increase in the amount of
282 Pr55^{Gag} in the cytoplasm did not result in an increase in the amount of Pr55^{Gag} in the supernatant,
283 as the amount of p24 in the supernatant was similar for cells with and without MG132 treatment
284 (Fig. 5B, compare second white and gray bars). The efficiency of Pr55^{Gag} release was, therefore,
285 almost halved (Fig. 5C, second gray bar). Thus, a wild type level of Pr55^{Gag} in the cells treated
286 with PIP5K1 α siRNA and MG132 is not sufficient to counteract the absence of PI(4,5)P₂ in the
287 membrane, emphasizing the essential role of this recognition during viral budding. Conversely,
288 the amounts of Pr55^{Gag} present in the cytoplasm (Fig. 5A) and supernatant of PIP5K1 γ -depleted
289 cells (Fig. 5B) were similar in the presence and absence of MG132 treatment. Pr55^{Gag} release
290 efficiency thus remained low in the presence of the proteasome inhibitor (Fig. 5C, fourth gray
291 bar). This result, together with the lack of Pr55^{Gag} and LysoTracker colocalization (Fig. 4),
292 indicates that an absence of PIP5K1 γ -mediated PI(4,5)P₂ production does not seem to induce
293 Pr55^{Gag} hydrolysis.

294 Overall, these results show that PIP5K1 β is dispensable for Pr55^{Gag} release, whereas PIP5K1 α
295 and PIP5K1 γ are both involved in Pr55^{Gag} release. In addition to decreasing release efficiency,
296 our results indicate that the depletion of PIP5K1 α has a critical effect on cytoplasmic Pr55^{Gag}
297 levels.

298

299 **Discussion**

300 The inner leaflet of the PM, which is enriched in PI(4,5)P₂, is targeted by Pr55^{Gag} at late stages
301 of the replication cycle. In this study, we determined the role of each PIP5K1 isoform in the
302 cellular localization of Pr55^{Gag} and its accumulation at the assembly site in TZM-bl HeLa cells,
303 a well-characterized model for studies of the HIV-1 replication cycle. Using a semi quantitative
304 UHPLC-HRMS² approach, we showed that the knockdown of PIP5K1 isoforms decreased
305 PI(4,5)P₂ levels to various extents (Fig. 1D and Fig. 2). The siRNA-based approach used here

306 did not completely eliminate PI(4,5)P₂ from the cells, probably due to the well-described
307 redundancy of production pathways (18, 33, 34). Consistent with the data shown in Fig. 1A,
308 indicating that PIP5K1 α is the principal isoform produced (in terms of the amount of mRNA),
309 we showed that this isoform is also the principal isoform underlying total PI(4,5)P₂ production
310 in TZM-bl HeLa cells (Fig. 1D). We identified 13 molecular species of PI(4,5)P₂ with different
311 fatty acyl chain compositions in TZM-bl HeLa cells. The principal phosphoinositide species
312 are known to carry C20:4/18:0 acyl chains (35–37), but our findings show that C20:2/C18:0 is
313 the major PI(4,5)P₂ species in TZM-bl HeLa cells, followed by C18:1/C18:0 and C18:1/C18:1
314 (Fig. 2). Similar results have been reported for several transformed cell lines, and the low
315 abundance of the C20:4/18:0 species is thought to be due to the culture medium used (38–41).
316 Our results suggest that molecular species bearing C20:1/C18:0; C18:1/C18:0; C22:2/C18:0
317 and C20:2/C18:0 could be the principal species generated by PIP5K1 α activity, suggesting the
318 specificity of PIP5K1 isoforms for certain PI(4,5)P₂ species, consistent with previous *in vitro*
319 studies in which PI(4)P was used as a substrate (42, 43).

320 The sequential depletion of PIP5K1 isoforms performed here revealed, for the first time, the
321 importance of the isoforms PIP5K1 α and γ , and the corresponding PI(4,5)P₂ metabolism, for
322 the cellular trafficking of Pr55^{Gag}. Based on the effects of the depletion of PIP5K1 α and γ , a
323 relationship between PI(4,5)P₂ metabolism and Pr55^{Gag} localization was established. Pr55^{Gag}
324 expression in TZM-bl HeLa cells leads to the accumulation of the protein mainly at the PM,
325 although there is also some cytoplasmic labeling (Fig. 3A and 3C, rows a). The depletion of
326 PIP5K1 α results in a much lower level of Pr55^{Gag} accumulation at the PM (Fig. 3A and 3C,
327 rows b). This strong reduction may result from the decrease of PI(4,5)P₂ level at the membrane,
328 consistent with the known importance of PI(4,5)P₂ concentration for the PM targeting of
329 Pr55^{Gag} (6, 12). Consequently, Pr55^{Gag} is degraded by the proteasome (Fig. 5A) and/or by the
330 lysosomes (Fig. 4E) in PIP5K1 α -depleted cells. The MG132-mediated inhibition of Pr55^{Gag}

331 proteolysis restores cytoplasmic Pr55^{Gag} level (Fig 5A, lower panel) but not Pr55^{Gag} release
332 efficiency (Fig. 5C, second grey bar). Interestingly, the depletion of Arf6, an activator of
333 PIP5K1 α , also resulted in a lower expression of Pr55^{Gag} in HeLa cells (44). These findings
334 indicate that PIK5K α inhibition results in lower level of intracellular Pr55^{Gag} and a
335 significantly lower extracellular release of Pr55^{Gag}. Another study did not find any decrease of
336 HIV particles production in cells for which Arf6 was down regulated by siRNA (45). However,
337 mammary epithelial MCF-7 cells were used to produce the HIV particles, which could explain
338 the discrepancy in results. In our study, the ratio between the Pr55^{Gag} expression in the
339 supernatant and the total amount of Pr55^{Gag} expression (supernatant and lysate of PIP5K1 α -
340 depleted cells) is similar to that obtained with the non-targeting siRNA (Fig. 5C, compare first
341 and second white bars). This suggests that the residual level of P(4,5)P₂ generated by the β and
342 γ isoforms or by other pathways is sufficient for the targeting of at least some Pr55^{Gag} at the PM
343 (33, 34). Moreover, the PIP5K1 isoforms have been reported to homo- or heterodimerize (46),
344 and we cannot exclude a potential role of PIP5K1 α/γ heterodimers in rescuing this residual
345 level of PM-PI(4,5)P₂. This heterodimerization of the PIP5K1 isoforms and their specific
346 cellular distribution may also explain why almost 50% of cellular PI(4,5)P₂ were conserved in
347 cells treated with siRNAs targeting PIP5K1 β or PIP5K1 γ mRNAs (Fig 1D). In conclusion, the
348 silencing of PIP5K1 α , a protein located principally at the PM, where it controls membrane
349 events and actin dynamics (14, 17, 18, 47), decreases the PI(4,5)P₂ concentration, in turn
350 strongly reducing the release of Pr55^{Gag} from the cell.

351 The impact of the PI(4,5)P₂ generated by PIP5K1 γ on the intracellular fate of Pr55^{Gag} seems to
352 involve another mechanism. In PIP5K1 γ -depleted cells, much less Pr55^{Gag} accumulates at the
353 PM than in control cells (Fig. 3A and 3C, rows d), but Pr55^{Gag} is mostly targeted to intracellular
354 vesicles corresponding to late endosomes (Fig. 4C, image d). This retargeting of Pr55^{Gag} to late
355 endosomes seems to be similar to that observed in PIP5K1 α -depleted cells (Fig. 4 C, image

356 b). However, there are two key differences between PIP5K1 α and PIP5K1 γ . On one hand,
357 Pr55^{Gag} is not localized in lysosomes when the PIP5K1 γ level is decreased (Fig. 4E, image d)
358 and, on the other hand, the level of intracellular Pr55^{Gag} is not affected by PIP5K1 γ silencing
359 (Fig. 5A). Nevertheless, despite this cytoplasmic accumulation of Pr55^{Gag}, lower levels of PM
360 targeting result in lower levels of Pr55^{Gag} release (Fig. 5C). The accumulation of Pr55^{Gag} in late
361 endosomes might have also favored an alternative trafficking pathway to the PM, which,
362 however, does not rescue the release defect observed (48, 49). Thus, the depletion of
363 PIP5K1 γ has a profound impact on the cellular behavior of Pr55^{Gag} despite the moderate
364 contribution of this isoform to PI(4,5)P₂ production (Fig. 1D and Fig. 2). Furthermore, given
365 that the PIP5K1 α isoform, which is considered to be the principal producer of PI(4,5)P₂, is still
366 active in PIP5K1 γ -depleted cells, the observed defects seem to be related to local and specific
367 pools of PI(4,5)P₂ dependent on PIP5K1 γ activity, rather than total PI(4,5)P₂ levels.
368 Interestingly, PIP5K1 γ has been reported to display lipid kinase behavior in focal adhesion
369 compartments (23, 50), and a previously study showed that an intracellular compartment
370 referred to as a “focal adhesion-like structure” was essential for HIV assembly and budding in
371 monocyte-derived macrophages (51). Thus, since depriving cells of PIP5K1 γ disrupts the focal
372 adhesion plaque (52), we can speculate that it may in turn decrease Pr55^{Gag} release efficiency
373 (Fig. 5).

374 In summary, we have identified PIP5K1 α and PIP5K1 γ as new determinants required for
375 targeting the Pr55^{Gag} to the PM in TZM-bl HeLa cells. We demonstrated the mistargeting of
376 Pr55^{Gag} from the PM to internal cytoplasmic compartments when PIP5K1 α and γ are silenced.
377 Further investigations are underway to determine whether these PIP5K1 isoforms acts similarly
378 in other cell models such as CD4 T cells or macrophages where the molecular determinants
379 directing Pr55^{Gag} assembly to virus-containing compartments may be different (53, 54).

380

381 **Acknowledgements**

382 This study was financially supported by a grant from the “Region Centre - Val de Loire”
383 (CalViC project, number 201500103990).

384

385 **Materials and Methods**

386 **Plasmids.**

387 Constructs encoding PIP5K1 α and PIP5K1 β were kindly provided by Yungfeng Feng (55).
388 Plasmids encoding GFP-PIP5K1 γ 90 (22300 and 22299 (56)) and mCherry-labeled Rab5 and
389 Rab7A (49201 (57) and 61804 (58)) were purchased from Addgene. The construction of human
390 codon-optimized plasmids encoding Pr55^{Gag}, Pr55^{Gag-eGFP} and Pr55^{Gag-mCherry} has been described
391 elsewhere (59, 60). The HIV-1 proviral DNA (pNL4-3) was (59, 60) obtained through the NIH
392 AIDS Reagent Program, Division of AIDS, NIAID.

393

394 **Antibodies.**

395 The anti-PIP5K1 α (C17, sc-11774), anti-HPRT (FL-218, sc-20975) and anti- β -actin antibodies
396 (I19, sc-1616) were purchased from Santa Cruz Biotechnology. The anti-PIP5K1 β
397 (ab1544818), anti-PIP5K1 γ (ab109192) and anti-HIV1p24 (ab53841) antibodies were
398 purchased from Abcam. The HRP-conjugated donkey anti-goat (6420-05), and donkey anti-
399 rabbit (6440-05) secondary antibodies were purchased from Southern Biotech, and the rabbit
400 anti-goat secondary antibody (ab6741) was obtained from Abcam.

401

402 **siRNA and siRNA transfection.**

403 All ON-TARGETplus RNA oligonucleotides and non-targeting control siRNAs (D-001810-
404 01-05) were obtained from Thermo Scientific Dharmacon. The siRNA target sequences are as
405 follows: PIP5K1 α : 5'-AAAUCAGUGAGGGCUCGCCUA-3' and 5'-

406 UUGAAAGGUGCCAUCCAGUUAGGC3-', PIP5K1 β : 5'-UGUUGGGAAUUCAUUCCUGGA-3' and 5'-
407 CAGCAAAGGGUUACCUCCAGUUCA-3', PIP5K1 γ : 5'-AUCAUCAAGACCGUCAUGCAC-3' and 5'-
408 GCCACCUUCUUUCGAAGAA-3' (61–63). For siRNA transfection, 2.5×10^5 TZM-bl HeLa cells
409 were cultured in a six-well plate and transfected with 100 pmol of a pool of two siRNA
410 sequences per isoform, with Lipofectamine RNAiMAX used according to the reverse protocol
411 of the manufacturer (Invitrogen). Flow cytometry analyses showed that around 80% of cells
412 were transfected when a fluorescently labeled siRNA (GLO-siRNA, Invitrogen) was used to
413 check the transfection efficiency (data not shown).

414

415 **Cell culture, transfection and Pr55^{Gag} release assays.**

416 TZM-bl HeLa cells (obtained through the NIH AIDS Reagent Program, Division of AIDS,
417 NIAID) were maintained in high-glucose pyruvate-supplemented DMEM, with 10% fetal calf
418 serum, 25 mM HEPES and gentamicin (50 μ g/ml).

419 For live-cell imaging, 2×10^5 TZM-bl HeLa cells were cultured in 35-mm imaging dish (Ibidi)
420 and transfected with siRNA as described above. After two days, cells were transfected with 0.8
421 μ g of plasmid encoding wild type Pr55^{Gag} and 0.2 μ g of plasmid encoding Pr55^{Gag-eGFP}, with or
422 without plasmids encoding mCherry-Rab5 or mCherry-Rab7A (ratio of 1:0.25:0.075), in the
423 presence of jetPEI (Ozyme), according to the manufacturer's instructions. The Pr55^{Gag}
424 assembly obtained with the mixture of plasmids encoding wild type Pr55^{Gag} and Pr55^{Gag-eGFP},
425 mixed in a ratio of 1:0.25, has been shown to resemble the wild-type virus in terms of Pr55^{Gag}
426 localization and particle morphology (59, 64, 65). The cells were mixed with 1 ml of phenol-
427 free DMEM imaging medium 24 h after DNA transfection. For PM staining, cells were washed
428 twice with phenol-free Opti-MEM medium and incubated with 1 ml of phenol-free medium
429 containing 15 nM of dSQ12S probe (a gift from Andrey Klymchenko, Strasbourg). The
430 incubation time was kept for 30 minutes, to minimize the entry of the dSQ12S probe and the

431 staining of intracellular membranes (28). Alternatively, the Pr55^{Gag-eGFP}-encoding plasmid was
432 replaced with a plasmid encoding Pr55^{Gag-mCherry} in the transfection mix, and LysoTracker
433 Green DND-26 (7526; Invitrogen) was used to stain acidic vesicles. The colors were then
434 inverted with ImageJ to facilitate interpretation of the images obtained.

435 To quantify the efficiency of Pr55^{Gag} release, Pr55^{Gag} expression levels were measured in the
436 cell supernatants by ELISA (Innotest HIV Antigen mAb, Fujirebio) and in the cell lysates by
437 Western blotting (see below). The cells were treated or not with the proteasome inhibitor
438 MG132 (Sigma-Aldrich). MG132 was used at a final concentration of 10 μ M and incubated for
439 6 h before cell lysis. The amounts of Pr55^{Gag} found in the supernatant and the lysate of cells
440 transfected with the non-targeting control siRNA were given the arbitrary value of 1. The levels
441 of Pr55^{Gag} in the supernatants and in the lysates of PIP5K1-depleted cells were expressed
442 relative to this value of 1. Pr55^{Gag} release efficiency was then calculated by dividing the amount
443 of Pr55^{Gag} found in the supernatant by the total amount of Pr55^{Gag} (supernatant and lysate) and
444 expressed as percentage compared to control cells transfected with non-targeting siRNA.

445

446 **Microscopy.**

447 Live-cell imaging was performed at 37°C, with 5% CO₂, and a Leica TCS SP8 g-STED 3X
448 inverted confocal microscope equipped with a 63 \times 1.4NA oil immersion objective (HXC PL
449 APO 63x/1.40 OIL CS) (Leica). The analysis of the entire cell was performed by a z-stack
450 acquisition. We obtained eGFP images by scanning the cells with a 488 nm laser line and a
451 500-555 nm band-pass filter for emission. The PM was detected, after incubating the cells with
452 the dSQ12S probe for 30 min, with excitation at 632 nm and the use of a 640-750 nm band-
453 pass filter for emission. For the mCherry images, a 558 nm laser line was used with a 605-730
454 nm band-pass filter.

455

456 **SDS-PAGE and Western blot analysis.**

457 Proteins were isolated with the NucleoSpin®RNA/protein kit (Macherey-Nagel), and the
458 protein pellet was then solubilized in protein solubilizing buffer containing Tris 2-
459 carboxyethyl-phosphine (PSB-TCEP), in accordance with the manufacturer's protocol. The
460 total amount of protein was determined with a DS-11 spectrophotometer (DeNovix). Proteins
461 were then denatured by heating and analyzed by SDS-PAGE in 8 to 16% polyacrylamide gels
462 (Eurogentec). The protein bands obtained were transferred onto membranes, which were then
463 probed with primary antibodies followed by the appropriate HRP-conjugated secondary
464 antibodies diluted in blocking solution (50 mM TBS, 0.05% Tween, 5% milk powder).
465 Membranes were incubated with the Pierce ECL substrate (Thermo Scientific) and the signals
466 were acquired with the ImageQuant LAS 500 system and analyzed with ImageQuant TL8.1
467 (GE Healthcare) or ImageJ software.

468

469 **RT-qPCR.**

470 Total RNA was isolated with the NucleoSpin®RNA/protein kit (Macherey-Nagel) according
471 to the manufacturer's instructions. We subjected 1 µg of total RNA to reverse transcription with
472 the SuperScript III First-Strand Synthesis System (Invitrogen). The synthesized cDNA was then
473 used for qPCR with the LightCycler® 480 SYBR Green I Master system (Roche) and the
474 following primers: PIP5K1α: forward-GAACGGTTCAGCGCTTCAT reverse-
475 GTCTCTCCAACACTAGAGGTGA, PIP5K1β: forward-CCAGGAATGGAAGGATGAGA reverse-
476 AATTGTGGTTGCCAAGGAAG, PIP5K1γ: forward-GCTACTTCCGGGAGCTCTTT reverse-
477 CGTAGAAGAGGGAGCCACTG, HPRT1: forward-TGACCTTGATTTATTTTGCATAC reverse-
478 CGAGCAAGACGTTTCAGTCCT. The data were analyzed with LightCycler 480 software (Roche)
479 and normalized to that of hypoxanthine phosphoribosyltransferase 1 (HPRT1) mRNA.

480 Absolute quantification was achieved by comparing the cycle threshold (CT) values of our
481 samples to those of a range of standards.

482

483 **Lipid extraction and LC-MS analysis.**

484 For PI(4,5)P₂ quantification, we transfected 5×10⁵ TZM-bl HeLa cells with siRNA as described
485 above. Seventy-two hours post-transfection, cells were scraped into 1 ml of 1 M HCl at 4°C
486 and centrifuged (15,000 x g, 5 min, 4°C). Pellets were resuspended in a mixture of
487 methanol/CHCl₃/1 M HCl (52.6/26.2/2.6%) in water, with PI(4)P-diC16 and PI(4,5)P₂-diC16
488 (Tebu-bio) added as internal standards. After addition of CHCl₃/2 M HCl (80/20%) and
489 centrifugation (1,500 x g, 5 min at room temperature), the organic phase was collected. The
490 solvent was then evaporated with a SpeedVac at 35°C and the residues were resuspended in
491 500 µL of methanol. A derivatization step was performed by adding 50 µl of CH₂N₂ followed
492 by an incubation at room temperature for 30 minutes. This operation was done twice. Finally,
493 the reaction was stopped by adding 10 µl of acetic acid. The reaction mixture was evaporated,
494 and the residues were resuspended in 100 µl of CH₃CN/H₂O (10% / 90%). Twenty-five
495 microliters of each sample was then injected for LC-MS analysis using a UHPLC Dionex™
496 Ultimate 3000 (Waters Acquity UPLC BEH300 C4 column, 45°C) with 0.1% formic acid in
497 water as phase A and 0.1% formic acid in CH₃CN as phase B, at a flow rate of 0.26 mL/min.
498 Gradient phase was as follows: 0-5 min: 100% of A, 5-8 min: 80% to 55% of A, 8-25 min: 55%
499 to 30 % of A, 25-30 min: 30% to 100% of A, 30-32.5 min: 100% of A, 32.5 to 37 min: 0% of
500 A. LC was coupled to a Q-Exactive mass spectrometer (Thermo Scientific) equipped with a
501 heated electrospray ionization source (HESI). The HESI parameters in positive polarity were
502 as follows: sheath gas flow rate: 35; auxiliary gas flow rate: 10; sweep gas flow rate: 1; spray
503 voltage: 3.50 kV; capillary temperature: 350°C; S-lens RF level: 60.0; heater temperature:
504 250°C. The full-scan acquisition parameters were as follows: resolution: 70,000; AGC target:

505 1e6; max IT: 100 ms; scan range: 850–1300. The parameters of top 10 data dependent MS² were
506 as follows: resolution: 35,000; isolation window: 1.0 *m/z*; collision energy: 20; AGC target:
507 1e6; max IT: 200 ms. Identification of each lipid was done based on the retention time
508 associated to high resolution full MS parent ion and confirmed by high resolution MS²
509 acquisition. Distinction between PIP and PIP₂ was realized based on neutral loss of each lipid
510 family. Chain lengths were determined based on mass fragment obtained during MS²
511 experiments. MS and MS² of each PIP and PIP₂ are available upon request. For each identified
512 lipid, chromatographic peak areas were obtained using Excalibur processing setup (Thermo
513 Fisher). Internal standards peak areas were used to normalize the amounts of each lipid. PI(4)P-
514 diC16 internal standard was used to normalized PIP lipids and PI(4,5)P₂-diC16 for PIP₂ lipids.
515 This normalization step was done by dividing signal intensity by that of the appropriate internal
516 standard. Semi-quantitative results are thus obtained and enable comparisons between samples.

517

518 **Statistical and image analysis.**

519 All our data were analyzed in non-parametric Mann-Whitney tests. The distribution of Pr55^{Gag-}
520 ^{eGFP} and its colocalization with the dSQ12S probe and mCh-Rab7A were quantitatively
521 analyzed from the two-color confocal images obtained with the “Squassh” plugin in ImageJ
522 software (29). The “Squassh” method allows images segmentation and quantification of the
523 distribution, size and intensity of transmitted signals. Therefore, the software delineates the
524 fluorescent object in each channel and calculates their overlap. The software provides then the
525 Pearson correlation coefficient accounting for the colocalization of the different markers in each
526 condition. We followed step by step the protocol previously described by Rizk *et al.* (29). The
527 software generates the *R* script “*R_analysis*”. *R* was used to perform one-way ANOVA for the
528 statistical analysis of differences between datasets. The distribution of Pr55^{Gag-mCherry} and its
529 colocalization with the LysoTracker Green probe were evaluated by the same method.

530 **Bibliography**

- 531 1. Hermida-Matsumoto L, Resh MD. 2000. Localization of human immunodeficiency virus
532 type 1 Gag and Env at the plasma membrane by confocal imaging. *J Virol* 74:8670–
533 8679.
- 534 2. Freed EO. 2015. HIV-1 assembly, release and maturation. *Nat Rev Microbiol* 13:484–
535 496.
- 536 3. Bryant M, Ratner L. 1990. Myristoylation-dependent replication and assembly of human
537 immunodeficiency virus 1. *Proc Natl Acad Sci* 87:523–527.
- 538 4. Gottlinger HG, Sodroski JG, Haseltine WA. 1989. Role of capsid precursor processing
539 and myristoylation in morphogenesis and infectivity of human immunodeficiency virus
540 type 1. *Proc Natl Acad Sci U S A* 86:5781–5785.
- 541 5. Zhou W, Parent LJ, Wills JW, Resh MD. 1994. Identification of a membrane-binding
542 domain within the amino-terminal region of human immunodeficiency virus type 1 Gag
543 protein which interacts with acidic phospholipids. *J Virol* 68:2556–69.
- 544 6. Ono A, Ablan SD, Lockett SJ, Nagashima K, Freed EO. 2004. Phosphatidylinositol (4,5)-
545 bisphosphate regulates HIV-1 Gag targeting to the plasma membrane. *Proc Natl Acad*
546 *Sci U S A* 101:14889–94.
- 547 7. Shkriabai N, Datta SAK, Zhao Z, Hess S, Rein A, Kvaratskhelia M. 2006. Interactions
548 of HIV-1 Gag with assembly cofactors. *Biochemistry* 45:4077–4083.
- 549 8. Chukkapalli V, Hogue IB, Boyko V, Hu W-S, Ono A. 2008. Interaction between the
550 human immunodeficiency virus type 1 Gag matrix domain and phosphatidylinositol-
551 (4,5)-bisphosphate is essential for efficient Gag membrane binding. *J Virol* 82:2405–
552 2417.
- 553 9. Chan R, Uchil PD, Jin J, Shui G, Ott DE, Mothes W, Wenk MR. 2008. Retroviruses
554 human immunodeficiency virus and murine leukemia virus are enriched in

- 555 phosphoinositides. *J Virol* 82:11228–11238.
- 556 10. Saad JS, Miller J, Tai J, Kim A, Ghanam RH, Summers MF. 2006. Structural basis for
557 targeting HIV-1 Gag proteins to the plasma membrane for virus assembly. *Proc Natl*
558 *Acad Sci* 103:11364–11369.
- 559 11. Mercredi PY, Bucca N, Loeliger B, Gaines CR, Mehta M, Bhargava P, Tedbury PR,
560 Charlier L, Floquet N, Muriaux D, Favard C, Sanders CR, Freed EO, Marchant J,
561 Summers MF. 2016. Structural and molecular determinants of membrane binding by the
562 HIV-1 matrix protein. *J Mol Biol* 428:1637–1655.
- 563 12. Mücksch F, Laketa V, Müller B, Schultz C, Kräusslich H-G. 2017. Synchronized HIV
564 assembly by tunable PIP2 changes reveals PIP2 requirement for stable Gag anchoring.
565 *Elife* 6:1–26.
- 566 13. Tang C, Loeliger E, Luncsford P, Kinde I, Beckett D, Summers MF. 2004. Entropic
567 switch regulates myristate exposure in the HIV-1 matrix protein. *Proc Natl Acad Sci U*
568 *S A* 101:517–522.
- 569 14. Doughman RL, Firestone AJ, Anderson RA. 2003. Phosphatidylinositol phosphate
570 kinases put PI4,5P₂ in its place. *J Membr Biol* 194:77–89.
- 571 15. Mellman DL, Gonzales ML, Song C, Barlow CA, Wang P, Kendziorski C, Anderson
572 RA. 2008. A PtdIns4,5P₂-regulated nuclear poly(A) polymerase controls expression of
573 select mRNAs. *Nature* 451:1013–1017.
- 574 16. Boronenkov I V., Loijens JC, Umeda M, Anderson RA. 1998. Phosphoinositide
575 signaling pathways in nuclei are associated with nuclear speckles containing Pre-mRNA
576 processing factors. *Mol Biol Cell* 9:3547–3560.
- 577 17. Honda A, Nogami M, Yokozeki T, Yamazaki M, Nakamura H, Watanabe H, Kawamoto
578 K, Nakayama K, Morris AJ, Frohman M a, Kanaho Y. 1999. Phosphatidylinositol 4-
579 phosphate 5-kinase α is a downstream effector of the small G protein ARF6 in membrane

- 580 ruffle formation. *Cell* 99:521–532.
- 581 18. Balla T. 2013. Phosphoinositides: Tiny lipids with giant impact on cell regulation.
582 *Physiol Rev* 93:1019–1137.
- 583 19. Brown FD, Rozelle AL, Yin HL, Balla T, Donaldson JG. 2001. Phosphatidylinositol 4,5-
584 bisphosphate and Arf6-regulated membrane traffic. *J Cell Biol* 154:1007–1017.
- 585 20. Schill NJ, Anderson RA. 2009. Two novel phosphatidylinositol-4-phosphate 5-kinase
586 type Iγ splice variants expressed in human cells display distinctive cellular
587 targeting. *Biochem J* 422:473–82.
- 588 21. van den Bout I, Divecha N. 2009. PIP5K-driven PtdIns(4,5)P₂ synthesis: Regulation and
589 cellular functions. *J Cell Sci* 122:3837–3850.
- 590 22. Oude Weernink PA, Schmidt M, Jakobs KH. 2004. Regulation and cellular roles of
591 phosphoinositide 5-kinases. *Eur J Pharmacol* 500:87–99.
- 592 23. Ling K, Doughman RL, Firestone AJ, Bunce MW, Anderson RA. 2002. Type Iγ
593 phosphatidylinositol phosphate kinase targets and regulates focal adhesions. *Nature*
594 420:89–93.
- 595 24. Akiyama C, Shinozaki-Narikawa N, Kitazawa T, Hamakubo T, Kodama T, Shibasaki Y.
596 2005. Phosphatidylinositol-4-phosphate 5-kinase gamma is associated with cell-cell
597 junction in A431 epithelial cells. *Cell Biol Int* 29:514–20.
- 598 25. Wang YJ, Li WH, Wang J, Xu K, Dong P, Luo X, Yin HL. 2004. Critical role of
599 PIP5KIγ87 in InsP₃-mediated Ca²⁺ signaling. *J Cell Biol* 167:1005–1010.
- 600 26. Volpicelli-Daley LA, Lucast L, Gong L-W, Liu L, Sasaki J, Sasaki T, Abrams CS,
601 Kanaho Y, De Camilli P. 2010. Phosphatidylinositol-4-phosphate 5-kinases and
602 phosphatidylinositol 4,5-bisphosphate synthesis in the brain. *J Biol Chem* 285:28708–
603 28714.
- 604 27. Hoppe A. 2012. What mRNA abundances can tell us about metabolism. *Metabolites*

- 605 2:614–631.
- 606 28. Karpenko IA, Collot M, Richert L, Valencia C, Villa P, Mély Y, Hibert M, Bonnet D,
607 Klymchenko AS. 2015. Fluorogenic squaraine dimers with polarity-sensitive folding as
608 bright far-red probes for background-free bioimaging. *J Am Chem Soc* 137:405–412.
- 609 29. Rizk A, Paul G, Incardona P, Bugarski M, Mansouri M, Niemann A, Ziegler U, Berger
610 P, Sbalzarini IF. 2014. Segmentation and quantification of subcellular structures in
611 fluorescence microscopy images using Squassh. *Nat Protoc* 9:586–596.
- 612 30. Zerial M, Parton R, Chavrier P, Frank R. 1992. Localization of Rab family members in
613 animal cells. *Methods Enzymol* 219:398–407.
- 614 31. Wandinger-Ness A, Zerial M. 2014. Rab proteins and the compartmentalization of the
615 endosomal system. *Cold Spring Harb Perspect Biol* 6:a022616–a022616.
- 616 32. Ochiai H, Sakai S, Hirabayashi T, Shimizu Y, Terasawa K. 1995. Inhibitory effect of
617 bafilomycin A1, a specific inhibitor of vacuolar-type proton pump, on the growth of
618 influenza A and B viruses in MDCK cells. *Antiviral Res* 4:425–30.
- 619 33. Vicinanza M, D'Angelo G, Di Campli A, De Matteis MA. 2008. Function and
620 dysfunction of the PI system in membrane trafficking. *EMBO J* 27:2457–2470.
- 621 34. Burke JE. 2018. Structural basis for regulation of phosphoinositide kinases and their
622 involvement in human disease. *Mol Cell* 71:653–673.
- 623 35. Pettitt TR, Dove SK, Lubben A, Calaminus SDJ, Wakelam MJO. 2006. Analysis of
624 intact phosphoinositides in biological samples. *J Lipid Res* 47:1588–96.
- 625 36. Milne SB, Ivanova PT, DeCamp D, Hsueh RC, Brown HA. 2005. A targeted mass
626 spectrometric analysis of phosphatidylinositol phosphate species. *J Lipid Res* 46:1796–
627 1802.
- 628 37. D'Souza K, Epand RM. 2014. Enrichment of phosphatidylinositols with specific acyl
629 chains. *Biochim Biophys Acta - Biomembr* 1838:1501–1508.

- 630 38. Ogiso H, Taguchi R. 2008. Reversed-phase LC/MS method for polyphosphoinositide
631 analyses: Changes in molecular species levels during epidermal growth factor activation
632 in A431 cells. *Anal Chem* 80:9226–9232.
- 633 39. Clark J, Anderson KE, Juvin V, Smith TS, Karpe F, Wakelam MJO, Stephens LR,
634 Hawkins PT. 2011. Quantification of PtdInsP 3 molecular species in cells and tissues by
635 mass spectrometry. *Nat Methods* 8:267–272.
- 636 40. Rouzer CA, Ivanova PT, Byrne MO, Milne SB, Marnett LJ, Brown HA. 2006. Lipid
637 profiling reveals arachidonate deficiency in RAW264.7 cells: Structural and functional
638 implications †. *Biochemistry* 45:14795–14808.
- 639 41. Traynor-Kaplan A, Kruse M, Dickson EJ, Dai G, Vivas O, Yu H, Whittington D, Hille
640 B. 2017. Fatty-acyl chain profiles of cellular phosphoinositides. *Biochim Biophys Acta*
641 - *Mol Cell Biol Lipids* 1862:513–522.
- 642 42. Shulga Y V., Anderson RA, Topham MK, Epand RM. 2012. Phosphatidylinositol-4-
643 phosphate 5-kinase isoforms exhibit acyl chain selectivity for both substrate and lipid
644 Activator. *J Biol Chem* 287:35953–35963.
- 645 43. Shulga Y V., Topham MK, Epand RM. 2011. Study of arachidonoyl specificity in two
646 enzymes of the PI cycle. *J Mol Biol* 409:101–112.
- 647 44. Joshi A, Garg H, Nagashima K, Bonifacino JS, Freed EO. 2008. GGA and Arf proteins
648 modulate retrovirus assembly and release. *Mol Cell* 30:227–238.
- 649 45. Ghossoub R, Lembo F, Rubio A, Gaillard CB, Bouchet J, Vitale N, Slavík J, Machala
650 M, Zimmermann P. 2014. Syntenin-ALIX exosome biogenesis and budding into
651 multivesicular bodies are controlled by ARF6 and PLD2. *Nat Commun* 5:445–56.
- 652 46. Lacalle RA, De Karam JC, Martínez-Muñoz L, Artetxe I, Peregil RM, Sot J, Rojas AM,
653 Goñi FM, Mellado M, Mañes S. 2015. Type I phosphatidylinositol 4-phosphate 5-kinase
654 homo and heterodimerization determines its membrane localization and activity. *FASEB*

655 J 29:2371–2385.

656 47. Doughman RL, Firestone AJ, Wojtasiak ML, Bunce MW, Anderson RA. 2003.
657 Membrane ruffling requires coordination between type I phosphatidylinositol phosphate
658 kinase and Rac signaling. *J Biol Chem* 278:23036–23045.

659 48. Booth AM, Fang Y, Fallon JK, Yang J-M, Hildreth JEK, Gould SJ. 2006. Exosomes and
660 HIV Gag bud from endosome-like domains of the T cell plasma membrane. *J Cell Biol*
661 172:923–935.

662 49. Kemler I, Meehan A, Poeschla EM. 2010. Live-cell coimaging of the genomic RNAs
663 and Gag proteins of two lentiviruses. *J Virol* 84:6352–6366.

664 50. Ling K, Schill NJ, Wagoner MP, Sun Y, Anderson RA. 2006. Movin' on up: the role of
665 PtdIns(4,5)P(2) in cell migration. *Trends Cell Biol* 16:276–84.

666 51. Pelchen-Matthews A, Giese S, Mlčochová P, Turner J, Marsh M. 2012. β 2 Integrin
667 adhesion complexes maintain the integrity of HIV-1 assembly compartments in primary
668 macrophages. *Traffic* 13:273–291.

669 52. Wu Z, Li X, Sunkara M, Spearman H, Morris AJ, Huang C. 2011. PIPKI γ regulates focal
670 adhesion dynamics and colon cancer cell invasion. *PLoS One* 6:e24775.

671 53. Inlora J, Chukkapalli V, Bedi S, Ono A. 2016. Molecular determinants directing HIV-1
672 Gag assembly to virus-containing compartments in primary macrophages. *J Virol*
673 90:8509–19.

674 54. Joshi A, Ablan SD, Soheilian F, Nagashima K, Freed EO. 2009. Evidence that productive
675 human immunodeficiency virus type 1 assembly can occur in an intracellular
676 compartment. *J Virol* 83:5375–5387.

677 55. Kisseleva M, Feng Y, Ward M, Song C, Anderson RA, Longmore GD. 2005. The LIM
678 protein Ajuba regulates phosphatidylinositol 4,5-bisphosphate levels in migrating cells
679 through an interaction with and activation of PIPKI alpha. *Mol Cell Biol* 25:3956–66.

- 680 56. Di Paolo G, Pellegrini L, Letinic K, Cestra G, Zoncu R, Voronov S, Chang S, Guo J,
681 Wenk MR, De Camilli P. 2002. Recruitment and regulation of phosphatidylinositol
682 phosphate kinase type 1 γ by the FERM domain of talin. *Nature* 420:85–89.
- 683 57. Friedman JR, Webster BM, Mastronarde DN, Verhey KJ, Voeltz GK. 2010. ER sliding
684 dynamics and ER–mitochondrial contacts occur on acetylated microtubules. *J Cell Biol*
685 190:363–375.
- 686 58. Rowland AA, Chitwood PJ, Phillips MJ, Voeltz GK. 2014. ER contact sites define the
687 position and timing of endosome fission. *Cell* 159:1027–1041.
- 688 59. El Meshri SE, Dujardin D, Godet J, Richert L, Boudier C, Darlix JL, Didier P, Mély Y,
689 De Rocquigny H. 2015. Role of the nucleocapsid domain in HIV-1 gag oligomerization
690 and trafficking to the plasma membrane: A fluorescence lifetime imaging microscopy
691 investigation. *J Mol Biol* 427:1480–1494.
- 692 60. Muller B, Daecke J, Fackler OT, Dittmar MT, Zentgraf H, Krausslich H-G. 2004.
693 Construction and characterization of a fluorescently labeled infectious human
694 immunodeficiency virus type 1 derivative. *J Virol* 78:10803–10813.
- 695 61. Micucci F, Capuano C, Marchetti E, Piccoli M, Frati L, Santoni A, Galandrini R. 2008.
696 PI5KI-dependent signals are critical regulators of the cytolytic secretory pathway. *Blood*
697 111:4165–4172.
- 698 62. Xu Q, Zhang Y, Xiong X, Huang Y, Salisbury JL, Hu J, Ling K. 2014. PIPKI targets to
699 the centrosome and restrains centriole duplication. *J Cell Sci* 127:1293–1305.
- 700 63. Padrón D, Wang YJ, Yamamoto M, Yin H, Roth MG. 2003. Phosphatidylinositol
701 phosphate 5-kinase I β recruits AP-2 to the plasma membrane and regulates rates of
702 constitutive endocytosis. *J Cell Biol* 162:693–701.
- 703 64. Hübner W, Chen P, Del Portillo A, Liu Y, Gordon RE, Chen BK. 2007. Sequence of
704 human immunodeficiency virus type 1 (HIV-1) Gag localization and oligomerization

705 monitored with live confocal imaging of a replication-competent, fluorescently tagged
706 HIV-1. J Virol 81:12596–607.

707 65. Müller B, Daecke J, Fackler OT, Dittmar MT, Zentgraf H, Kräusslich H-G. 2004.
708 Construction and characterization of a fluorescently labeled infectious human
709 immunodeficiency virus type 1 derivative. J Virol 78:10803–13.

710

711 **Legends**

712 **FIG. 1. The silencing of PIP5K1 isoforms decreases PI(4,5)P₂ production.**

713 TZM-bl HeLa cells were transfected with either a non-targeting control siRNA or with siRNAs
714 targeting PIP5K1 α , PIP5K1 β or PIP5K1 γ . Data were collected 72 h after siRNA transfection.

715 (A) The silencing of each PIP5K1 isoforms was assessed by RT-qPCR measurements of the
716 corresponding mRNA expression, on the basis of comparison with the non-targeting control
717 siRNA. The absolute number of PIP5K1 mRNA copies was determined by comparison with a
718 range of standards, with normalization against HPRT1 mRNA as an internal control. (B) The
719 knockdown of PIP5K1 proteins was assessed by Western blotting, with HPRT1 proteins used
720 to verify protein loading between lanes. (C) The impact of silencing a single PIP5K1 isoform
721 on the two others was assessed by RT-qPCR, on the basis of comparison with the non-targeting
722 control siRNA, as described previously for A. (D) The effect of each PIP5K1 isoform silencing
723 on total cellular PI(4,5)P₂ level was determined by UHPLC-HRMS². For panels A, C and D,
724 the data shown are expressed as the mean \pm the standard error of the mean (SEM) from three
725 independent experiments performed in triplicate. The p values shown were obtained with
726 Mann-Whitney tests for panels A, C and D. Significant results (**** for p value < 0.0001, ***
727 0.0001 < p value < 0.001, ** 0.001 < p value < 0.01, * 0.01 < p value < 0.05, ns = not significant)
728 are indicated.

729

730 **FIG. 2. The knockdown of PIP5K1 isoforms has various effects on the distribution of**
731 **PI(4,5)P₂ species.**

732 Lipids were extracted from the lysate of TZM-bl HeLa cells three days after transfection with
733 either a non-targeting control siRNA or with siRNAs targeting PIP5K1 α , PIP5K1 β or PIP5K1 γ .
734 The effect of PIP5K1 isoform silencing on the distribution of PI(4,5)P₂ molecular species was
735 assessed by UHPLC-HRMS². The histogram shows the response ratio of each PI(4,5)P₂
736 molecular species area peak from the lysate of cells transfected with the non-targeting control
737 siRNA (black bars) or an siRNA targeting PIP5K1 α , β or γ (blue, gray and green bars,
738 respectively). The data shown are the means and SEM of three independent experiments
739 conducted in triplicate. Mann-Whitney tests were performed to assess the significance of
740 differences. Significant results (**** for p value < 0.0001, *** 0.0001 < p value < 0.001, ** 0.001
741 < p value < 0.01, * 0.01 < p value < 0.05, ns = not significant) are indicated. Stars indicate a
742 significant decrease in the amount of a particular molecular species relative to the basal amount
743 present in control cells. The stars above the black lines indicate significant differences in
744 amounts of molecular species between siRNA-PIP5K1 α -transfected cells and the cells
745 transfected with other siRNAs.

746

747 **FIG. 3. The knockdown of PIP5K1 α and PIP5K1 γ impairs HIV-1 Pr55^{Gag} localization to**
748 **the plasma membrane.**

749 TZM-bl HeLa cells, transfected with either a non-targeting control siRNA or with siRNAs
750 targeting each PIP5K1 isoform, were then transfected with plasmids expressing
751 Pr55^{Gag}/Pr55^{Gag-eGFP} or with a replication-competent HIV provirus plasmid pNL4.3 and a
752 Pr55^{Gag-eGFP} expressing plasmid. One day after transfection, the PM of the cells were stained
753 with the dSQ12S probe and living cells were imaged by confocal microscopy. (A) Effect of
754 PIP5K1 isoform silencing on the distribution of Pr55^{Gag} in transfected cells. Representative z-

755 stack images (green for Pr55^{Gag}, red for the dSQ12S probe and yellow for the merged channels)
756 for cells transfected with non-targeting control siRNA or siRNA targeting PIP5K1 α , PIP5K1 β
757 or PIP5K1 γ (a, b, c and d, respectively) are shown. (B) The colocalization of Pr55^{Gag} with the
758 PM probe (dSQ12S) was quantified with ImageJ software. Each dot represents the average of
759 R for 10 z-stack images of a cell. Horizontal black bars stand for the mean value. (C) Effect of
760 PIP5K1 isoforms silencing on the distribution of Pr55^{Gag} produced by the replication-competent
761 HIV-1_{NL4.3} in transfected cells. Representative z-stack images (green for Pr55^{Gag}, red for the
762 dSQ12S probe and yellow for the merged channels) from cells transfected with non-targeting
763 control siRNA or siRNAs targeting PIP5K1 α , PIP5K1 β or PIP5K1 γ (a, b, c and d, respectively)
764 are shown. (D) The colocalization of Pr55^{Gag} produced by the replication-competent HIV-
765 1_{NL4.3} with the PM probe dSQ12S was quantified with ImageJ software. Each dot represents
766 the average of R for 10 z-stack images of a cell. Horizontal black bars stand for the mean value.
767 Mann-Whitney tests were performed to assess the significance of differences. Significant
768 results (**** p value < 0.0001, ns = not significant) are indicated.

769

770 **FIG. 4. The silencing of PIP5K1 α and PIP5K1 γ has different effects on the retargeting of**
771 **HIV-1 Pr55^{Gag} to endosomal pathways.**

772 (A) Effect of the silencing of PIP5K1 isoforms on the rerouting of Pr55^{Gag} to early endosomes.
773 TZM-bl HeLa cells, transfected with either a non-targeting control siRNA or with siRNAs
774 targeting each PIP5K1 isoform, were then transfected with plasmids encoding Pr55^{Gag}/Pr55^{Gag}-
775 eGFP and mCh-Rab5. Z-stack confocal images were acquired from living cells as previously
776 described. Representative yellow merged images (green for Pr55^{Gag} and red for mCh-Rab5) are
777 shown for cells transfected with non-targeting control siRNA or siRNA targeting PIP5K1 α ,
778 PIP5K1 β or PIP5K1 γ (a, b, c and d, respectively). (B) The colocalization of Pr55^{Gag}-eGFP with
779 mCh-Rab5 was quantified with ImageJ software. Each dots represents the average of R for 10

780 z-stack images of a representative cell. Horizontal black bars stand for the mean value. (C)
781 Effect of the silencing of PIP5K1 isoforms on the rerouting of Pr55^{Gag} to late endosomes. TZM-
782 bl HeLa cells, transfected with either a non-targeting control siRNA or with siRNAs targeting
783 each PIP5K1 isoform, were then transfected with plasmids encoding Pr55^{Gag}/Pr55^{Gag-eGFP} and
784 mCh-Rab7A. Z-stack confocal images were acquired from living cells as previously described.
785 Representative yellow merged images (green for Pr55^{Gag} and red for mCh-Rab7A) are shown
786 for cells transfected with non-targeting control siRNA or siRNA targeting PIP5K1 α , PIP5K1 β
787 or PIP5K1 γ (a, b, c and d, respectively). (D) The colocalization of Pr55^{Gag-eGFP} with mCh-
788 Rab7A was quantified with ImageJ software. Each dots represents the average of *R* for 10 z-
789 stack images of a representative cell. Horizontal black bars stand for the mean value. (E) Effect
790 of PIP5K1 isoform silencing on the relocation of Pr55^{Gag} to acidic vesicles. TZM-bl HeLa
791 cells, transfected with either a non-targeting control siRNA or with siRNAs targeting each
792 PIP5K1 isoform, were cotransfected with Pr55^{Gag} and Pr55^{Gag-mCherry}-expressing plasmids.
793 Lysosomes were stained in green with the LysoTracker probe 24 h hours after DNA
794 transfection. Acquisitions of z-stack confocal images were performed as previously described
795 and the colors of Pr55^{Gag-mCherry} and the green LysoTracker probe were inversed to prevent
796 confusion. Representative yellow merged images (green for Pr55^{Gag} and red for the LysoTracker
797 probe) are shown for cells transfected with non-targeting control siRNA or siRNA targeting
798 PIP5K1 α , PIP5K1 β or PIP5K1 γ (a, b, c and d, respectively). (F) The colocalization of Pr55^{Gag-}
799 ^{mCherry} with the green LysoTracker probe was quantified with ImageJ software. Each dots
800 represents the average of *R* for 10 z-stack images of a representative cell. Horizontal black bars
801 stand for the mean value. Mann-Whitney tests were performed to assess the significance of
802 differences. Significant results (**** for p value < 0.0001, *** 0.0001 < p value < 0.001, ns =
803 not significant) are indicated.

804

805 **FIG. 5. Silencing of PIP5K1 α and PIP5K1 γ impairs Pr55^{Gag} targeting to PM and release**
806 **into the cell supernatant.**

807 TZM-bl HeLa cells, transfected with siRNA targeting the PIP5K1 isoforms, were then
808 transfected with a Pr55^{Gag}-encoding plasmid. One-day post transfection, cells were treated with
809 10 μ M of MG132. (A) The level of intracellular Pr55^{Gag} expression was analyzed by Western
810 blotting 48 h post transfection. The β -actin protein was used to normalize protein loading
811 between lanes. The bands in the top part of each panel correspond to the Pr55^{Gag} in siRNA-
812 transfected cells without (upper panel) or with MG132 (lower panel) treatment, and the results
813 shown are representative of three independent experiments (each in duplicate).
814 Chemiluminescence analysis was performed with ImageJ software to assess Pr55^{Gag} levels. The
815 red box highlights Pr55^{Gag} level in PIP5K1 α -depleted cells. (B) Pr55^{Gag} release in the
816 supernatant was assessed using an anti-p24 ELISA 48 h post transfection. The histogram shows
817 the mean and SEM of p24 concentration (ng/ml) in the supernatants of cells left untreated (white
818 bars) or treated with MG132 (gray bars) in three independent experiments. (C) Pr55^{Gag} release
819 efficiency was calculated as described in Materials and Methods, in three independent
820 experiments. This histogram shows the Pr55^{Gag} release efficiency of transfected TZM-bl HeLa
821 cells left untreated (white bars) or treated with MG132 (gray bars), expressed as percentage
822 compared to control cells transfected with the non-targeting siRNA. Mann-Whitney tests were
823 performed to assess the significance of differences. Significant results (**** p value < 0.0001;
824 ***, 0.0001 < p value < 0.001, ns = not significant) are indicated.

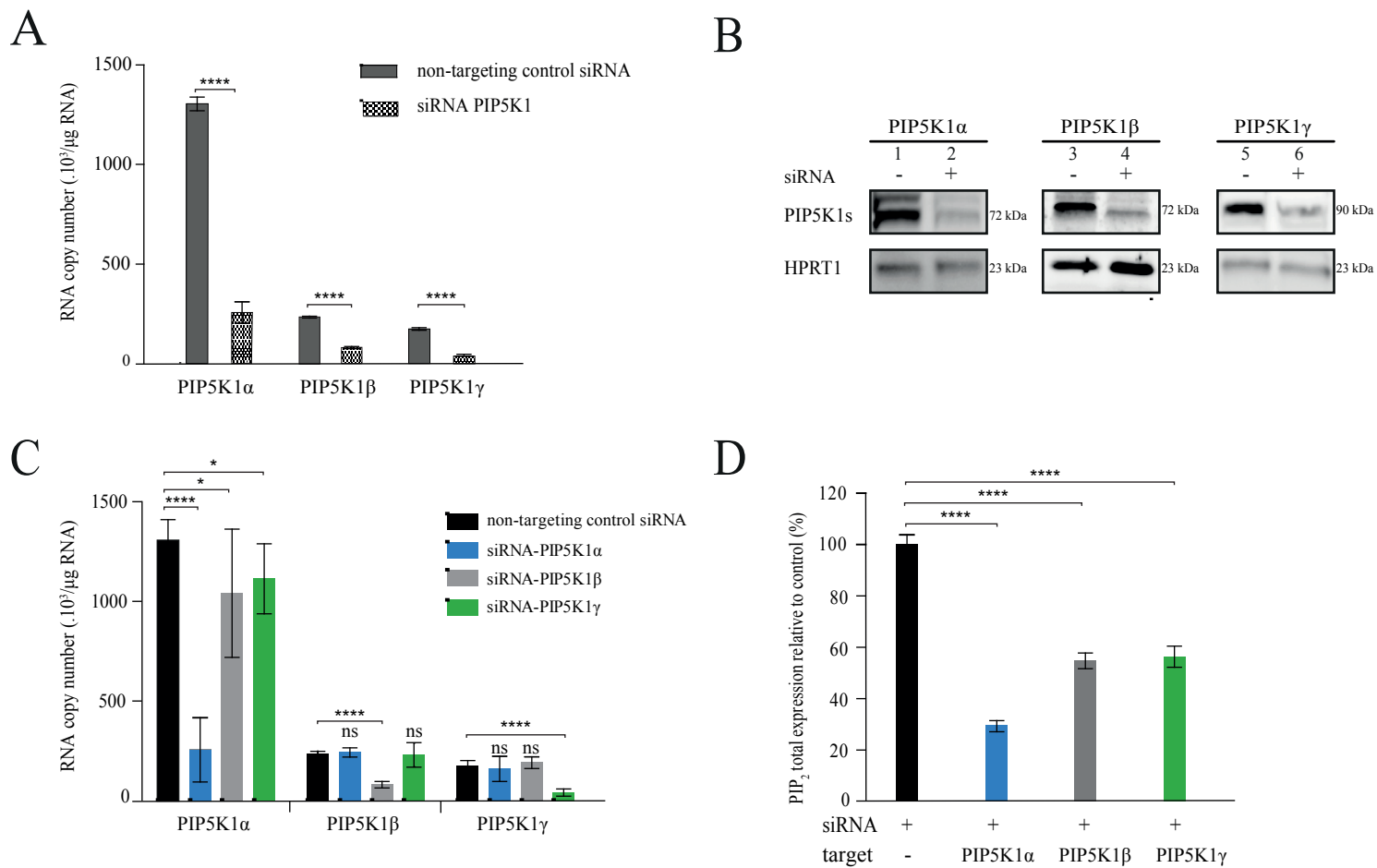


FIG. 1. The silencing of PIP5K1 isoforms decreases PI(4,5)P₂ production.

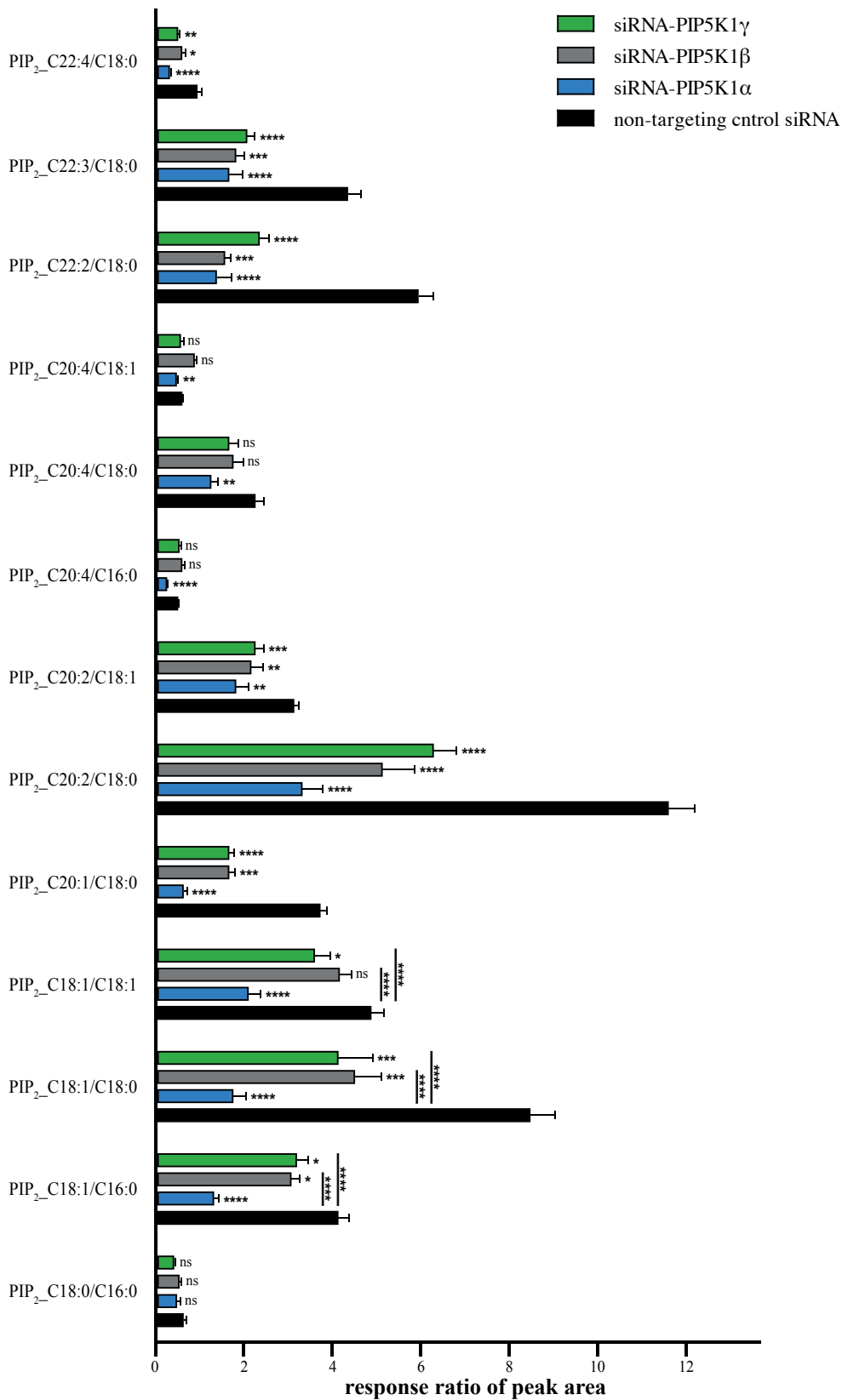


FIG. 2. The knockdown of PIP5K1 isoforms has various effects on the distribution of PI(4,5)P₂ species.

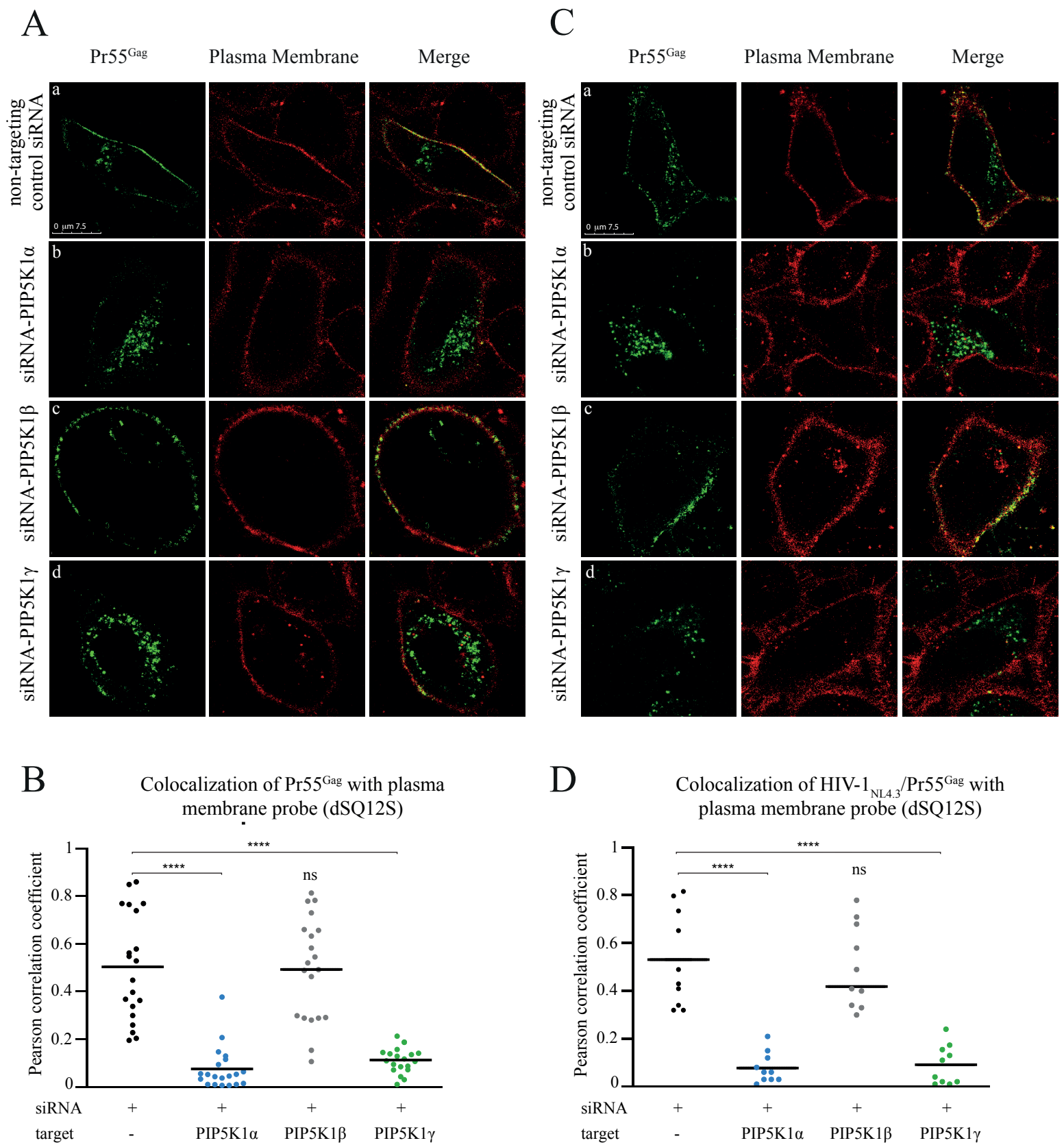
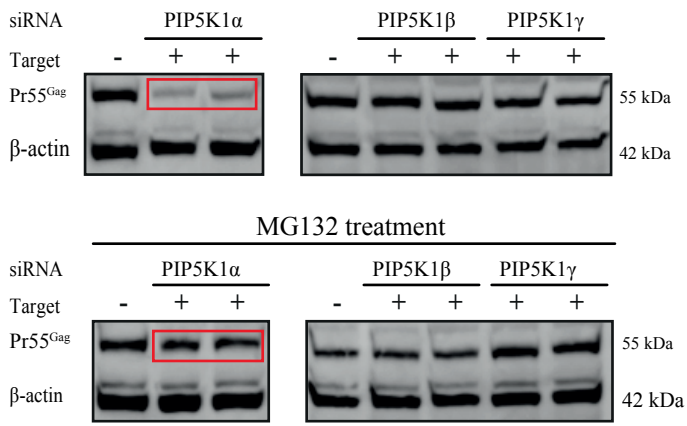
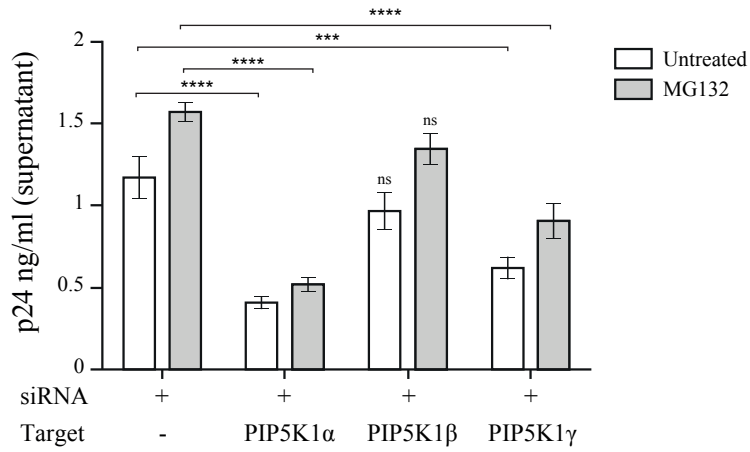


FIG. 3. The knockdown of PIP5K1 α and PIP5K1 γ impairs HIV-1 Pr55^{Gag} localization to the plasma membrane.

A



B



C

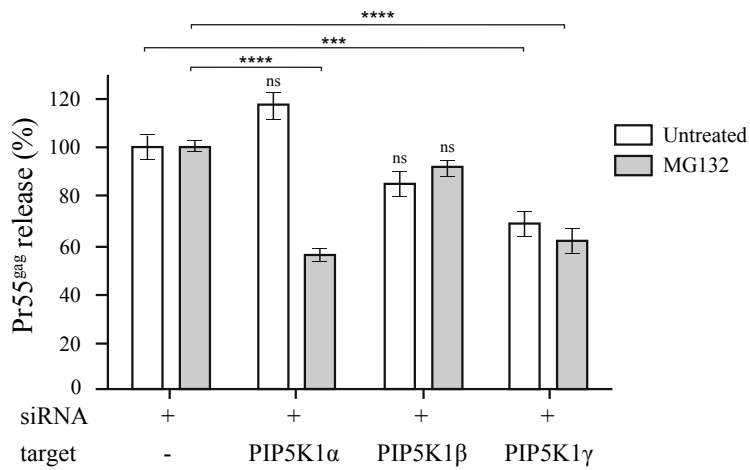


FIG. 5. Silencing of PIP5K1 α and PIP5K1 γ impairs Pr55^{Gag} targeting to PM and release into the cell supernatant.